Journal of Corrosion and Materials
www.corromat.com

J. Corros. Mater. (2026) 5(2), 259–269.

Hydrogen-Induced Hydroxylation and Defect-Controlled Weakening of Ti–6Al–4V Passive Films in Artificial Seawater

Louis E. Brus[1,*]

Department of Chemistry, Columbia University, New York, NY 10027, USA

*Corresponding author: leb26@columbia.edu

(Received: 23 August 2026. Received in revised form: 8 November 2026. Accepted: 19 November 2026. Published online: 30 December 2026.)

Abstract

Ti–6Al–4V alloy is selected for marine and offshore structures due to its high specific strength in conjunction with fast formation of a nanometric titanium-oxide passive film. At the same time, cathodic polarization in presence of chloride ions in seawater leads to generation of atomic hydrogen at the metal/electrolyte interface, its incorporation into the near-surface alloy structure, and change of the passive-layer chemistry and electronic defects population. This work investigates the influence of hydrogen charging on the state of the passive film on the Ti–6Al–4V alloy in artificial seawater for 0, 1, 4, 8, and 12 h. Composition of the alloy was 6.03 wt.% Al, 4.14 wt.% V, 0.01 wt.% C, 0.08 wt.% O, balance Ti, and the charging condition was pH 8.2 ± 0.1, $25 \pm 1\,^{\circ}\mathrm{C}$, cathodic current density of 20 mA cm^{-2}. The electrochemical impedance spectroscopy, potentiodynamic polarization, Mott-Schottky analysis of donor density, thickness of the passive film, and TiO_2/TiOOH surface fractions were used to analyze passivity deterioration during hydrogen formation. Polarization resistance decreased from 1.93×10^6 to $2.86 \times 10^5\,\Omega\,\mathrm{cm}^2$ after 12 h, whereas the corrosion current density increased from 4.62×10^{-8} to 9.19×10^{-8} A cm^{-2}. Donor density increased from 4.22×10^{19} to 6.10×10^{19} cm^{-3}, passive-film thickness decreased from 1.81 to 1.12 nm, TiO_2 content decreased from 93.86% to 86.18%, and TiOOH-related fraction increased from 6.14% to 13.82%. Passive-film integrity index decreased from 1.000 to 0.086, whereas barrier-disorder amplification factor increased from 1.000 to 38.996. This study shows that hydrogen charging influences passivation not only by thinning of the oxide film. It results in conversion of the dense TiO_2-dominated barrier into the hydroxylated, donor-defective, electrochemically heterogeneous film, which stays passive but allows more charge transfer.

Keywords: Ti–6Al–4V alloy; artificial seawater; hydrogen charging; passive film; TiO_2; TiOOH; electrochemical impedance spectroscopy; Mott–Schottky analysis; donor density; corrosion resistance.

1. Introduction

The use of titanium alloys in marine, offshore, biomedical, chemical processing, energy, and aerospace systems results from their high mechanical efficiency, low density, good fatigue resistance, and passivation in many neutral or oxidizing environments [1]. Ti–6Al–4V is the most common alloy among the $\alpha + \beta$ titanium alloy group; aluminium acts as a α phase stabilizer, vanadium as a β phase stabilizer, and phase balance is responsible for strength, toughness, machinability, and heat treatment [2]. In addition, general information on titanium alloys explains why titanium is preferred in high-performance structural applications [3]. In oxygenated seawater, the alloy is usually covered by a thin passive layer composed mainly of TiO_2, supplemented with titanium suboxides, hydroxylated titanium compounds, water adsorption, and oxygen-containing surface groups [4]. Medical and implants application also serve as an additional field for the discussion of passive film integrity [5]. Although the film thickness is about few nanometers, the film is responsible for low passive current density and high polarization resistance that makes titanium alloys attractive for chloride-containing environments.

Titanium alloy corrosion resistance is the result of passive film rather than intrinsic metallic nobility [6]. Repassivation ability of titanium is good enough to recover from many mechanical or chemical influences; the efficiency of repassivation depends on oxide compactness, stoichiometry, defect concentration, hydration, and metal/oxide interface integrity [7]. Low donor density oxide with TiO_2 dominates acts as a good barrier for ionic and electronic transport; hydrated or oxygen-deficient oxide may show higher charge transfer capability [8]. In chloride-containing seawater the distinction between compact and defective passive film is especially important due to the ability of chloride to use heterogeneity of passive film, hydrated oxide areas, and transport processes through defects [9]. According to general principles of corrosion prevention, the service behavior is the result of interaction of material, environment, and surface conditions [10]. Thus, corrosion-prevention design practice takes the protective film as a part of complex design system, not just a surface feature [11]. A titanium surface can be passive in general electrochemical sense but still loose the high-quality barrier capabilities for corrosion resistance.

Second corrosion problem is created by cathodic polarization. Marine parts may be subjected to cathodic protection, galvanic coupling, impressed currents, and oxygen depletion. These conditions hinder anodic dissolution, but create favorable conditions for hydrogen evolution. Hydrogen-assisted embrittlement is recognized as one of the structural damage processes in metallic materials [12]. Ti–6Al–4V is sensitive to hydrogen due to the hydrogen capability to diffuse through titanium alloy and accumulate at α/β interfaces, dislocations, grain boundaries, and hydride nucleation sites [13]. Metal-hydrogen interactions in general show the ability of hydrogen absorption to change bulk and near-surface properties [14]. Cathodic polarization may also induce hydride precipitation on the titanium surface [15]. The electrochemical effect of hydrogen

should be considered along with its mechanical effects, because hydrogen changes the near-surface properties of alloy which determines passive film formation.

The nanometric thickness of the passive film makes it sensitive to the hydrogen content. Accumulated hydrogen, hydride-related strain, local lattice expansion, and interface stress may disrupt the metal/oxide interface. The film can keep continuous morphology, but become less compact, hydrated, and conductive. This behavior cannot be assessed by passivity detection only. Coupled measurements including impedance resistance, current density, donor density, film thickness, and surface chemistry are needed. Hydrogen-assisted degradation of titanium passive film is considered in the present paper as the coupled process of surface-chemical and electrochemical processes.

EIS is a sensitive technique for identification of passive film deterioration before depassivation [16]. Polarization resistance R_p is a measure of overall resistance of surface to charge transfer and transport through the passive film. Polarization resistance method is commonly used for the estimation of corrosion rate and protective film change [17]. High R_p is the sign of compact and protective passive film; low R_p means weakening of the electrochemical barrier. The framework of electrochemical corrosion techniques helps to understand the connection of impedance, polarization, and surface reactions [18]. Constant-phase exponent n from impedance fitting characterizes interfacial non-ideality. Interpretation of the impedance response of electrodes with constant-phase element behavior requires special attention [19]. Values close to unity mean uniform capacitive interface; lower values correspond to broad distribution of relaxation times due to thickness, surface roughness, chemical and reaction site heterogeneities. Estimates of effective capacitance and film thickness become more reliable with explicit consideration of constant-phase-element behavior [20]. EIS was widely used for investigation of corrosion protection and interfacial degradation in protective coatings [21]. The theoretical basis for this interpretation lies in the fact that charge transfer, double-layer and diffusion effects can contribute to the impedance spectrum [22]. Combined decrease in R_p and n gives us the reason to conclude that hydrogen charging affects not only barrier resistance, but interfacial uniformity too.

Potentiodynamic polarization provides additional kinetic data. Corrosion current density i_{corr} characterizes the intensity of reaction near the corrosion potential; passive current density i_{pass} describes charge transfer through the film during passive polarization. Passive film of titanium usually shows low values of these parameters. Hydrogen charging may cause current increase due to film thinning, hydration, increased electronic conductivity, and local heterogeneity. Nevertheless, the increase in current density cannot fully characterize film degradation. Two-fold increase in i_{corr} has significant meaning but it acquires another value if it occurs simultaneously with 85% decrease in R_p, 44% increase in donor density, and substantial chemical conversion from TiO_2-related to TiOOH-related surface.

Mott-Schottky analysis gives us additional information about semiconductor properties of the passive film. Nanometric titanium passive layers can be characterized using photoelectrochemistry and semiconductor physics [23]. Passive films on titanium are generally n-type semiconductors, where donor-type defects originate from oxygen vacancies, Ti^{3+} ions, and related defects [24]. Point defect model explains the effect of defect formation and migration on passive film growth and transport processes [25]. Passive film electronic structure was shown to determine corrosion behavior in some alloy systems [26]. Thermodynamics of aqueous electrochemical equilibria can help in understanding of oxide stability and potential-dependent surface states [27]. Increase in donor density leads to higher electronic conductivity and weakens the capability of oxide to impede charge transfer. Thus, simultaneous increase in donor density with decrease in R_p and increase in i_{pass} means that film degradation cannot be caused by the film thinning alone. It corresponds to the change in the defect structure of the film.

Surface chemistry is the third factor in the film analysis. The major compact and stable component of titanium passivity is TiO_2. Thin titanium oxide films produced by anodization change their properties depending on formation conditions [28]. The structure and composition of anodic titanium oxide films also depend strongly on film formation conditions [29]. The link between chemistry and electrochemical resistance of titanium passive oxide films is evident from the impedance studies [30]. Long-time immersion of titanium oxide films in neutral solution can change their properties too [31]. Increased amount of TiOOH-related species means that the film is more hydroxylated, hydrated, and chemically disturbed. This may explain decreased resistance and increased passive current because hydrated areas can contain more structural and electronic disorder. The main goal of this study is to find out if the hydrogen charging of Ti–6Al–4V in artificial seawater causes mainly the film thinning or its transformation into hydroxylated and donor-defective transport film.

2. Material and Calculations

Titanium alloy Ti–6Al–4V containing 6.03 wt.% Al, 4.14 wt.% V, 0.01 wt.% C, 0.08 wt.% O, and remainder Ti was used in the experiment. This condition corresponds to the solution annealing procedure performed at 950 °C for 30 min and subsequent air cooling, thus obtaining the equiaxed $\alpha + \beta$ microstructure. The hydrogenation process was carried out in artificial seawater at pH 8.2 ± 0.1 and 25 ± 1 °C in the constant cathodic current density of 20 mA cm^{-2}. Five different charging times were selected: 0, 1, 4, 8, and 12 hours [32]. Schematic representation of the experimental setup and measurement channels are given in Fig. 1. The figure identifies the alloy composition, electrochemical charging environment, time sequence, and the four measurement groups used for interpretation: electrochemical impedance spectroscopy, polarization, Mott–Schottky analysis, and surface chemistry.

The arrangement of the photographs in Figure 1 is significant since the corrosion reaction depends on the interaction between the material condition, electrolyte composition, charge intensity, and time of exposure. The specimen is assessed through a sequence of charging processes rather than individual parameters. Condition 0 h stands for the passivated alloy in artificial seawater, while conditions 1, 4, 8, and 12 h stand for the increasingly higher hydrogen exposure under identical electrolyte temperature, pH, and current density. This sequential process enables the distinction between early-stage passive film disruption and late-stage chemical and semiconductor disorders.

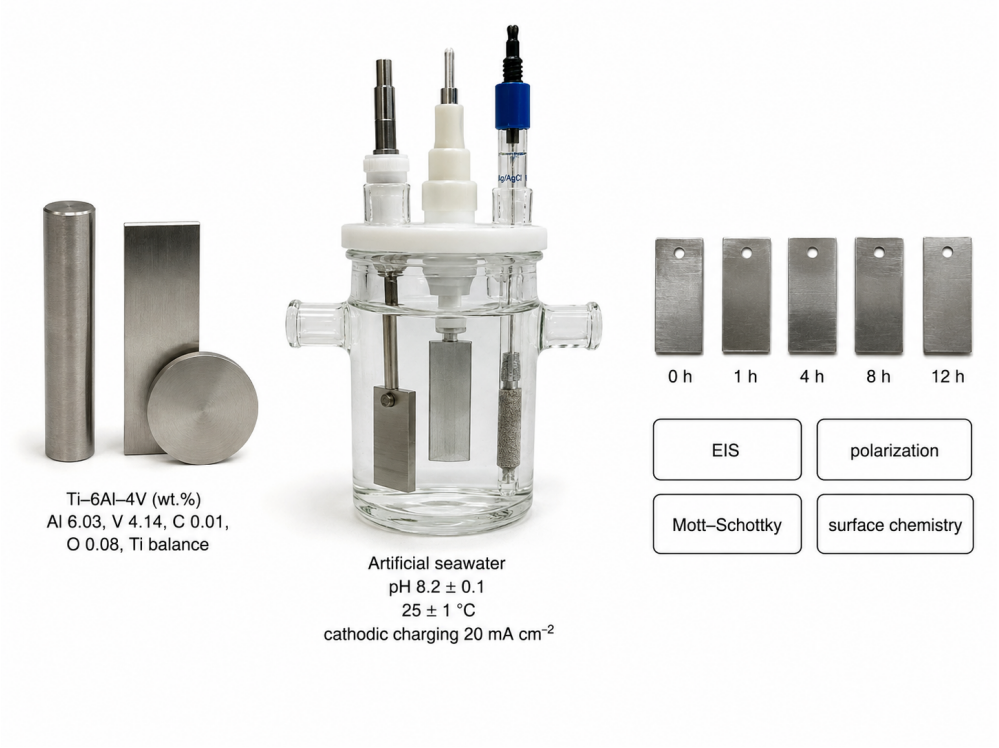

Figure 1: Artificial-seawater charging route.

The variables utilized in the equations include the polarization resistance R_p, constant-phase exponent n, apparent passive-film thickness d, corrosion current density i_{corr}, passive current density i_{pass}, donor density N_D, TiO_2 surface fraction, and TiOOH-containing surface fraction. These variables are shown in Table 1. Each parameter describes a distinct aspect of the passive condition. Resistance is electrochemical blocking capability; exponent n is interface uniformity; film thickness is transport length scale; current densities are charge-transfer intensity; donor density is semiconductor disorder; and TiO_2 and TiOOH fractions are compact oxide preservation and hydroxylation.

Table 1: Electrochemical and passive-film variables of Ti–6Al–4V after hydrogen charging in artificial seawater.

t (h)	R_p (Ω cm^2)	n	d (nm)	i_{corr} (A cm^{-2})	i_{pass} (A cm^{-2})	N_D (10^{19} cm^{-3})
0	1.93×10^6	0.93	1.81	4.62×10^{-8}	9.05×10^{-7}	4.22
1	1.73×10^6	0.91	1.80	4.98×10^{-8}	9.76×10^{-7}	4.54
4	1.36×10^6	0.89	1.76	5.32×10^{-8}	1.15×10^{-6}	4.73
8	8.23×10^5	0.89	1.64	6.35×10^{-8}	1.27×10^{-6}	4.91
12	2.86×10^5	0.85	1.12	9.19×10^{-8}	1.67×10^{-6}	6.10

The sense of the values shown in Table 1 is already evidence for coordinated degradation. The parameters responsible for retained passivity integrity, which are R_p, n, and d, diminish when the charging time becomes larger. The parameters responsible for charge transport and disorder, which are i_{corr}, i_{pass}, and N_D, grow. Therefore, it is obvious that the surface changes through several interdependent parameters; the hydrogen charging process makes the passive film unstable through physical thickness reduction, interfacial response, electrochemical transport, and semiconductor disorder.

The passive film chemical structure and derived passive state descriptors are given in Table 2. The passive film integrity parameter Φ combines retained resistance, retained constant phase response, retained TiO_2 chemistry and the inverse donor density growth. The integrity loss parameter L_Φ reflects the complementary loss of this state. Barrier-disorder amplification parameter Ψ combines corrosion current amplification, passive current amplification, donor density growth, resistance loss and TiO_2 depletion.

Table 2: Surface-film chemistry and derived passive-state indices.

t (h)	TiO_2 (%)	TiOOH-related phase (%)	$\Phi(t)$	$L_\Phi(t)$	$\Psi(t)$
0	93.86	6.14	1.000	0.000	1.000
1	92.92	7.08	0.807	0.193	1.409
4	91.40	8.60	0.586	0.414	2.390
8	90.52	9.48	0.338	0.662	5.457
12	86.18	13.82	0.086	0.914	38.996

The passive-film integrity index was calculated as

$$\Phi(t) = \left(\frac{R_p(t)}{R_p(0)}\right)\left(\frac{n(t)}{n(0)}\right)\left(\frac{X_{\mathrm{TiO_2}}(t)}{X_{\mathrm{TiO_2}}(0)}\right)\left(\frac{N_D(0)}{N_D(t)}\right), \tag{1}$$

where $X_{\mathrm{TiO_2}}$ is the TiO_2 fraction. The uncharged condition was normalized to $\Phi = 1$. A lower value indicates loss of combined resistance, interfacial uniformity, compact oxide chemistry, and low-defect character. The integrity loss factor was calculated as

$$L_\Phi(t) = 1 - \Phi(t). \tag{2}$$

This term does not imply physical disappearance of the passive film. It indicates that the remaining film is no longer equivalent to the uncharged compact TiO_2-rich layer.

The barrier-disorder amplification factor was calculated as

$$\Psi(t) = \frac{(i_{\mathrm{corr}}(t)/i_{\mathrm{corr}}(0))\,(i_{\mathrm{pass}}(t)/i_{\mathrm{pass}}(0))\,(N_D(t)/N_D(0))}{(R_p(t)/R_p(0))\,(X_{\mathrm{TiO_2}}(t)/X_{\mathrm{TiO_2}}(0))}. \tag{3}$$

The numerator represents increased electrochemical activity, passive-region charge transport, and donor-type defects. The denominator represents remaining electrochemical resistance and compact oxide chemistry. The hydroxylated-film fraction was also evaluated as

$$f_{\mathrm{TiOOH}}(t) = \frac{X_{\mathrm{TiOOH}}(t)}{X_{\mathrm{TiO_2}}(t) + X_{\mathrm{TiOOH}}(t)}. \tag{4}$$

Because the TiO_2 and TiOOH-related fractions sum to 100% in this surface-composition record, f_{TiOOH} directly follows the TiOOH percentage expressed as a fraction.

3. Results and Discussion

3.1 Passive film morphology and chemical conversion

The morphological and chemical evolution of the nanometric film is depicted in Figure 2. The cross-sectional structure of the plate reveals the five charging states along with the corresponding thickness values and TiO_2/TiOOH fractions. The barrier thinning proceeds from 1.81 nm at 0 h to 1.12 nm at 12 h. It is worth noticing that this transformation is not only a simple decrease in the film thickness. In particular, the TiO_2-rich fraction reduces from 93.86% to 86.18%, whereas the TiOOH-related fraction increases from 6.14% to 13.82%. Hence, the film undergoes changes in terms of its morphology and chemical composition.

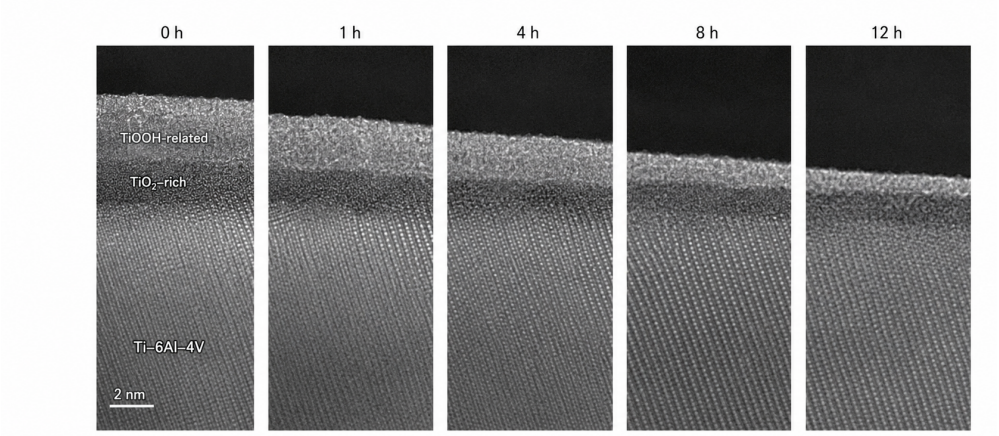

	0 h	1 h	4 h	8 h	12 h
Thickness (nm)	1.81	1.80	1.76	1.64	1.12
TiO_2 (%)	93.86	92.92	91.40	90.52	86.18
TiOOH (%)	6.14	7.08	8.60	9.48	13.82

Figure 2: Nanometric film conversion.

The series of images in Figure 2 demonstrates what is hidden behind the numerical data. Initially, the oxide film is a compact TiO_2-rich layer. After short charging, the thickness of the film does not change much, but the TiOOH-related fraction starts to grow. Finally, at 12 h, the film becomes thinner and more hydroxylated. This series of images clarifies why the alloy can be passive even when its barrier properties are significantly deteriorated. The hydroxylated film is no longer able to perform the barrier function due to the lack of compactness and chemical stability.

The chemical conversion is illustrated separately in Figure 3. The compositional ribbon shows clearly that TiO_2 depletion and TiOOH enrichment are two opposite processes. The TiO_2 fraction decreases by 7.68 percentage points after 12 h, whereas the TiOOH-related fraction grows by the same amount. The most noticeable changes take place between 8 h and 12 h, where the TiO_2 fraction decreases by 4.34 percentage points and the TiOOH-related fraction increases by 4.34 percentage

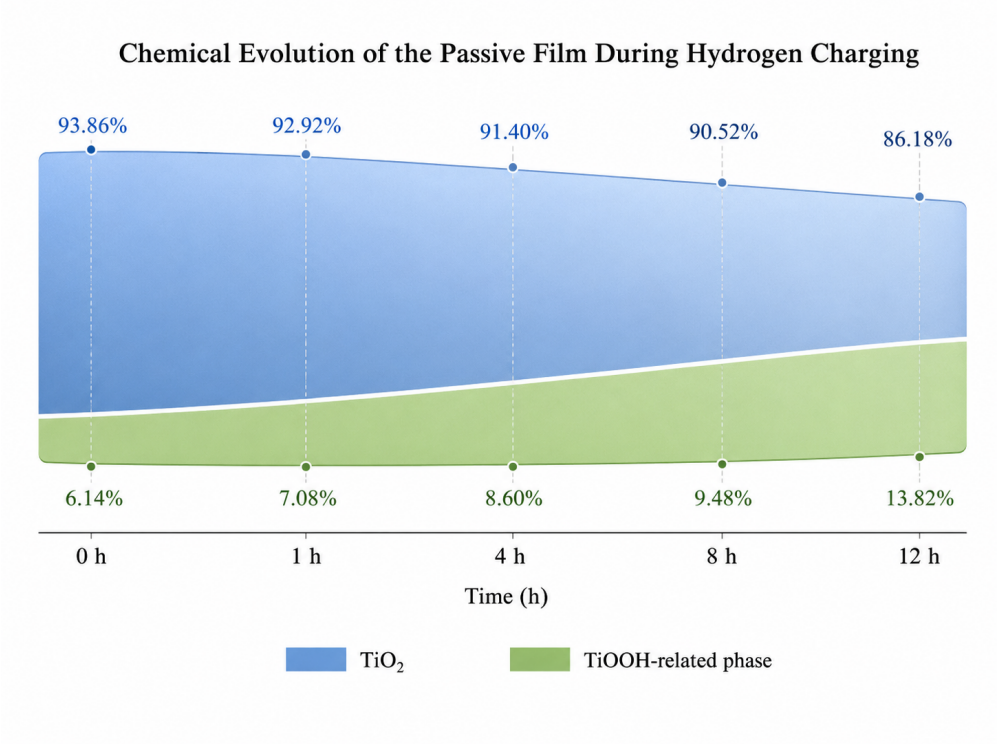

Figure 3: Oxide-to-oxyhydroxide shift.

points. It is the clearest indicator that long-duration hydrogen charging results in formation of another state of the oxide film, which differs from those obtained during the shorter charging periods.

The dependence presented in Figure 3 supports the idea that hydrogen-induced surface passivation deterioration is controlled by hydroxylation of the passive film. TiO_2 is the denser and more stable form that relates to high resistance, whereas TiOOH-related substance implies hydration and structural disorder. Doubling of the TiOOH-related content by 13.82% compared to 6.14% allows explaining the resistance drop, donor concentration rise, and current enhancement obtained during the electrical characterization of the sample. Thus, hydrogenation affects the chemical protection of the film instead of just changing its surface properties.

3.2 Electrochemical resistance and interfacial uniformity

The impedance-based resistance behavior is provided in Figure 4. The polarization resistance monotonically falls during charging time from $1.93 \times 10^6\,\Omega\,\mathrm{cm}^2$ at 0 h to $2.86 \times 10^5\,\Omega\,\mathrm{cm}^2$ at 12 h. It means that the 85.18% resistance loss occurs. The value of constant-phase exponent falls from 0.93 to 0.85 within this period. The n parameter drop is lower in magnitude compared to R_p but has physical significance because it demonstrates the growing degree of non-ideality and the broadening of distribution of interfacial relaxation times. From the behavior of both parameters depicted in Figure 4, it could be stated that the passive film is becoming less resistant and more non-uniform. Compact TiO_2 film is supposed to function as a high-resistance barrier having relatively ideal capacitive response. Hydrogen charging affects negatively on this behavior. The surface of the film charged for 12 hours is not equal to the uncharged passive film because the charge transfer is possible via other pathways which are less heterogeneous and more conductive. The n value decreasing from 0.93 to 0.85 agrees with the local film thickness variations, hydroxylation, influence of the hydride on the interfacial region, and non-uniform transport channels. The resistance loss is much higher than the thickness variation and cannot be considered as the reason for such behavior of the film. The film thickness drops by 38.12%, namely from 1.81 to 1.12 nm, while the polarization resistance drops by 85.18%. In case of geometrical thinning being the main factor of the resistance change, it would be expected to have the behavior of this quantity in correlation with the thickness variation. The large reduction in the resistivity indicates that the film has become increasingly electronically and chemically conductive. This is reinforced by the following discussions on the increase in the donor concentration and TiOOH content.

3.3 The response of current density in case of retained passivity

Figure 5 illustrates the normalized current density response. The corrosion current density increased from 4.62×10^{-8} to 9.19×10^{-8} A cm^{-2} in 12 hours, making the final ratio equal to 1.99. Passive current density increased from 9.05×10^{-7} to 1.67×10^{-6} A cm^{-2}, making the final ratio 1.85. As it follows from the increase in the currents, the hydrogen charging increased the electrochemical activity of the surface. However, their absolute values remained low as compared to active corrosion, but the importance of these changes lies in the fact that these changes were accompanied by a significant impedance loss.

The stepped representation illustrated in Figure 5 shows that the process started with a relatively low increase in the current and then continued with a strong late-stage current transport. During the first 4 hours, the ratio between

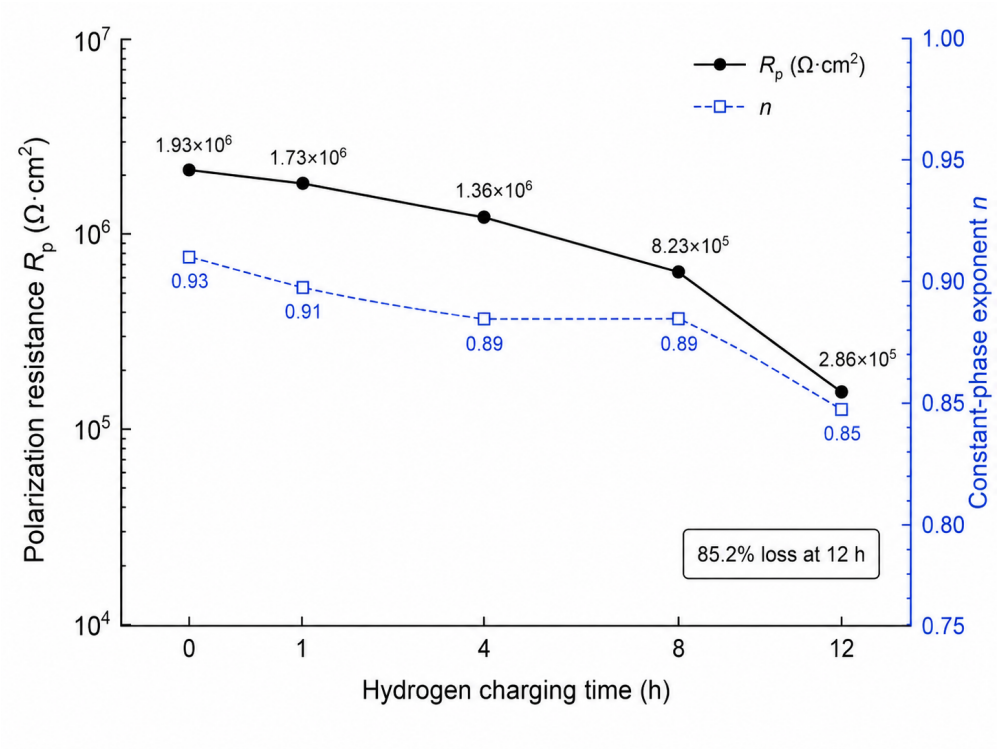

Figure 4: Barrier-resistance collapse.

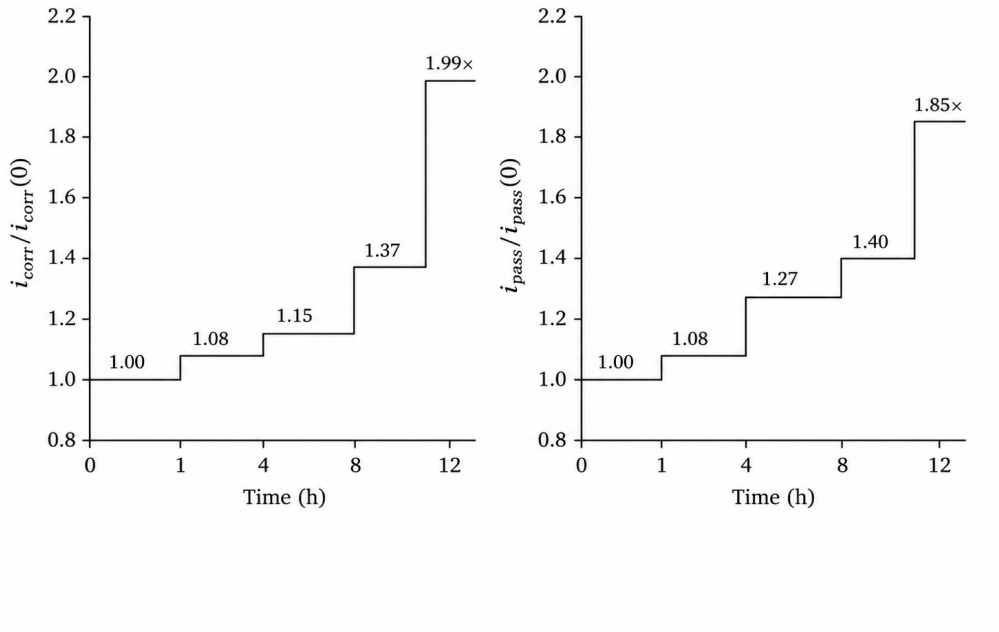

Figure 5: Current transport increase.

$i_{corr}/i_{corr}(0)$ was only 1.15, and the ratio between $i_{pass}/i_{pass}(0)$ was 1.27. After 8 hours, the corresponding ratios become 1.37 and 1.40, and after 12 hours, they are 1.99 and 1.85. The passive current response is especially significant for the case of Ti–6Al–4V since the passive current is the indicator of the charge transport through the protective film. Therefore, higher passive current density indicates the possibility of a higher charge transport during the anodic polarization due to the lower resistance and higher donor density.

The current density values should be analyzed jointly with other characteristics. The doubling of the corrosion current could be considered a moderate increase, especially taking into account that the absolute value of the current remained small. The same change becomes significantly higher in combination with the resistance loss of 85.18% and the decrease of Φ down to 0.086. The alloy is thus still nominally passive, but its passivity has been significantly compromised. This is especially relevant to marine materials, since low current density at a certain potential cannot ensure that the passive layer is chemically compact and electronically impervious.

3.4 Growth of donor density and thinning of the film

The relationship between donor density and film thickness is presented in Figure 6. It is seen from the evolution of tile series that there is an increase in defect density from 0 to 12 hours and reduction in film thickness. Thus, donor density grows from 4.22×10^{19} to 6.10×10^{19} cm^{-3}, which corresponds to 44.55% increase. Thickness falls from 1.81 to 1.12 nm. Both these factors act together, making the film become thinner and more electronically conducting.

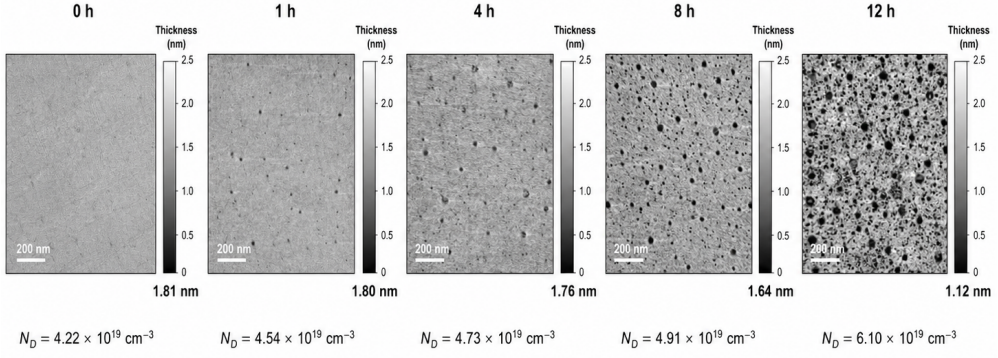

Figure 6: Defect density and thinning.

The visual evolution in Figure 6 is compatible with disorder in a titanium dioxide-based passive film from the point of view of n-type semiconductor. Defects, namely oxygen vacancies and states related to titanium ions in +3 oxidation state, increase conductivity of film and promote charge transferring. The donor density grows slowly during initial stages of charging and then increases considerably after 8 hours. So the value rises from 4.91×10^{19} cm^{-3} at 8 hours to 6.10×10^{19} cm^{-3} at 12 hours, which means late increase of 1.19×10^{19} cm^{-3}. This period provides the main part of donor-density increase.

Thus, the combination of donor density increase and film thickness fall explains the collapse of electrical resistance much stronger than thickness only can do it. Film becomes thinner, i.e. the transport distance becomes shorter and donor density grows, which means increase of electronic conductivity of this distance. Both these facts reinforce each other and provide a passive film, which is much weaker barrier. Such behavior is quite appropriate for point-defect model of passive film, where generation of defects determines transport across oxide layer [8]. Later works on point defects explain connection between passive film growth and degradation due to defect population [25]. The contribution of oxygen vacancies in anodic titanium oxide also supports the donor-density model used above [24].

3.5 Loss of integrity and barrier-disorder amplification

The index of passive film integrity provides a concise representation of the quality remaining in the film. Values of Φ drop from 1.000 at 0 h to 0.807 at 1 h, 0.586 at 4 h, 0.338 at 8 h, and 0.086 at 12 h. The complementary loss of integrity factor goes up from 0.000 to 0.914. This is demonstrated in Figure 7, where the retention-of-integrity curve shrinks while the loss band increases with charging time.

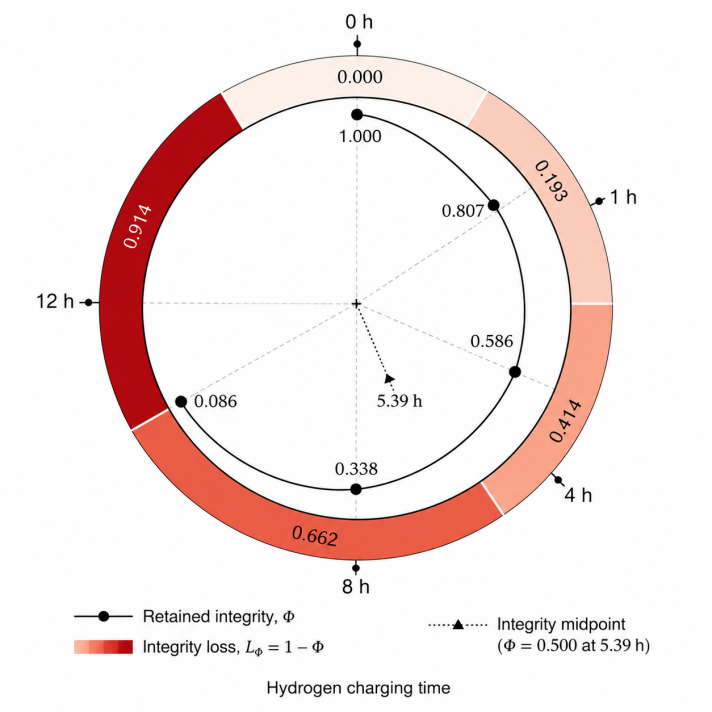

Figure 7: Passive integrity clock.

The timing-based representation in Figure 7 highlights the dynamics of passive film breakdown. By linear interpolation between 4 h and 8 h values, we get an integrity midpoint $\Phi = 0.5$ at approximately 5.39 h. Prior to this point, the passive film is disrupted but still retains more than half of the total resistance, uniformity, compact oxide, and defect-free properties. After this point, the film enters a lower-integrity regime. Value of $\Phi = 0.086$ at 12 h indicates that only a small portion of the normalized total quality of the passive film is left, despite the alloy not having entered the active dissolution regime yet.

The barrier-disorder amplification factor determines the degree of coupled breakdown. Values of Ψ grow from 1.000 at 0 h to 1.409 at 1 h, 2.390 at 4 h, 5.457 at 8 h, and 38.996 at 12 h. The interval contribution is presented in Figure 8. Interval 8-12 h is responsible for $\Delta\Psi = 33.539$, corresponding to 88.27% of the total rise from 0 to 12 h. Such late dominance of the process implies non-proportional dependence on charging time.

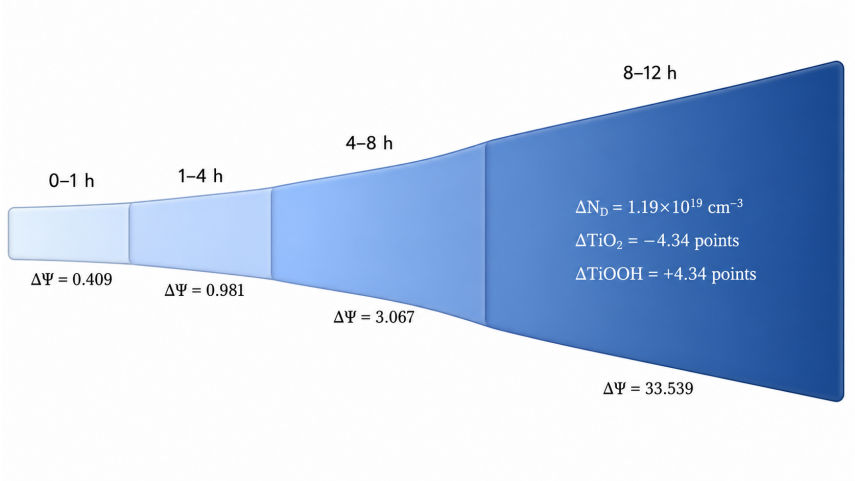

Figure 8: Late disorder dominance.

The widened final interval in Figure 8 allows us to determine the 8-12 h interval as the decisive transformation interval. The same interval includes an increase in the donor density of 1.19×10^{19} cm^{-3}, a TiO_2 decrease of 4.34 percentage points, and a TiOOH increase of 4.34 percentage points. These numbers indicate that the drastic rise in Ψ is caused not by one particular variable but rather by the simultaneous presence of current amplification, donor density growth, resistance loss, and chemical conversions.

The values of the intervals allow us to understand the relation between gradual and accelerated degradation. While the index of passive film integrity keeps decreasing across all intervals, the barrier-disorder amplification factor drastically rises only after 8 h. This indicates that the early charging stage leads to measurable weakening of the film, whereas long-term charging creates another state characterized by hydroxylation and electronic defects. The final state thus cannot be viewed as a mere extension of the earlier trend; it is a high-transport passive state.

The interval data in Table 3 make a connection between chemistry and electrochemistry in terms of numbers. Changes of Φ for the first two intervals are close to each other, while $\Delta\Psi$ for the third one is much higher. This allows concluding that in

Table 3: Interval changes during hydrogen charging.

Charging interval (h)	ΔTiO_2 (points)	ΔTiOOH (points)	ΔN_D (10^{19} cm^{-3})	$\Delta\Phi$	$\Delta\Psi$
0–1	-0.94	0.94	0.32	-0.193	0.409
1–4	-1.52	1.52	0.19	-0.221	0.981
4–8	-0.88	0.88	0.18	-0.248	3.067
8–12	-4.34	4.34	1.19	-0.252	33.539

the last stage, the film is influenced more by disorder amplification and not only integrity retention. High value of Ψ starting from 8 h happens due to increased film hydroxylation and electronic defectiveness while resistance continues to decrease.

3.6 Integrated passive-state interpretation

The full interpretation of the corrosion state is shown in Figure 9. State window plot divides the charging process into compact passive, transition passive, and high-disorder passive states. States 0 and 1 h belong to the compact passive area. State 4 h belongs to the transition area because Φ is decreased to 0.586 and Ψ is increased to 2.390. State 8 h belongs to the border with high-disorder passive area ($\Phi = 0.338$, $\Psi = 5.457$). Finally, state 12 h is placed in the high-disorder passive area with $\Phi = 0.086$, $\Psi = 38.996$, $R_p = 2.86 \times 10^5\,\Omega\,\mathrm{cm}^2$, and TiOOH = 13.82%.

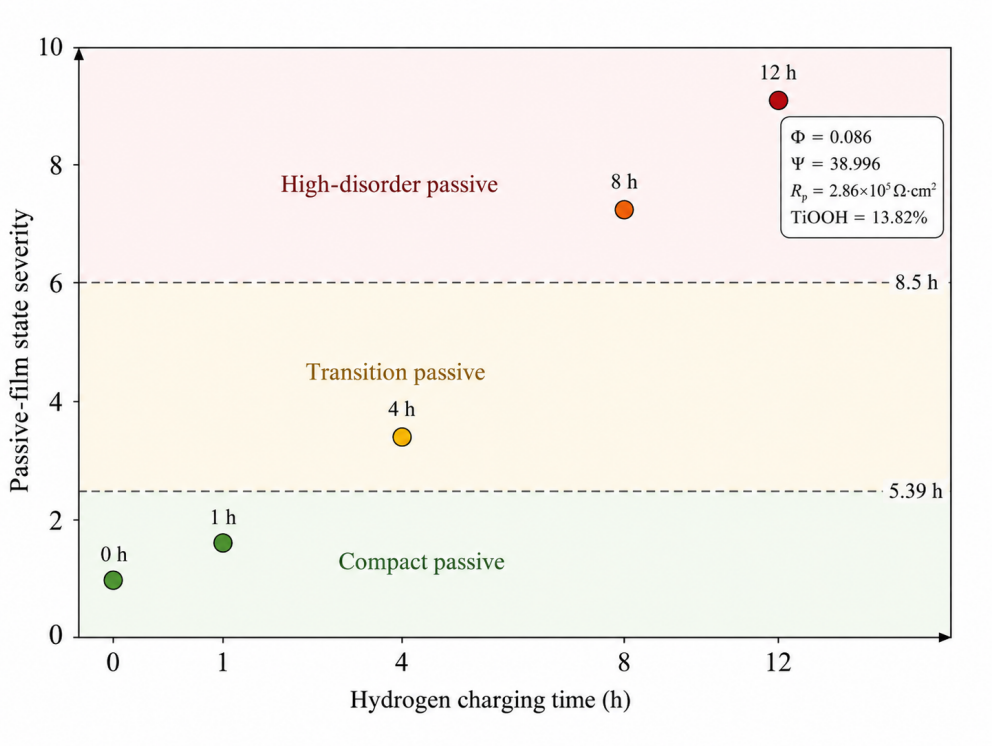

Figure 9: Hydrogen-damage state window.

This classification gives an answer to the most important materials question. The hydrogen charging of the surface does not immediately break the passivity but transforms the film from the compact passive state to the transition state and then to the high-disorder passive state. High-disorder passive state means passive film in the meaning that active dissolution is still restricted, but this is no longer a reliable compact passive film. This film contains higher donor density, lower TiO_2 fraction, increased TiOOH fraction, lower resistance, and higher current density.

It is clear from the state window that current density is not enough. Corrosion current density at 12 h is about 10^{-8} A cm^{-2}, so it can be considered as low corrosion activity. Integrated parameters show the seriousness of the situation. Passive film loses 91.4% of normalized combined integrity and shows disorder amplification of nearly 39. For the seawater application, this difference is significant since the low absolute value of current cannot exclude the chemically and electronically vulnerable to further transport film.

The mechanism derived from all figures above is coupled hydrogen–hydroxylation–defect mechanism. Cathodic charging leads to hydrogen formation at the interface of the alloy/electrolyte. Hydrogen enters the near-surface $\alpha + \beta$ alloy, which has phase boundaries, defects, and local trapping centers to keep hydrogen and create hydride-related interfacial stress. Since the passive film is nanometric, this disturbance influences the chemistry of oxide. TiO_2 fraction decreases, the fraction of TiOOH-related species increases, donor density increases, and film thickness decreases. It leads to the resistance decrease and passive region current transport increase.

The final 8–12 h interval is critical from the mechanistic point of view. During this interval, the TiOOH-related fraction increases from 9.48% to 13.82%, the donor density increases from 4.91×10^{19} to 6.10×10^{19} cm^{-3}, and Ψ increases from

5.457 to 38.996. This synchronous increase of the chemical and electronic disorder shows that hydrogen charging for a long period results in the passive film with a new transport characteristics. It is not only thinner, but more conductive, more hydrated, and more heterogeneous.

The engineering conclusion is straightforward. Cathodic protection and galvanic coupling decrease the anodic dissolution rate, but cathodic polarization for a long period might generate hydrogen and cause the degradation of the passive film. So, the titanium alloy components in seawater should be evaluated not only by corrosion current density but also by impedance resistance, passive current density, hydroxylation of the surface, and donor density response. The surface that retains high R_p, high n, high TiO_2 fraction, low TiOOH fraction, and low N_D growth after the cathodic exposure is more probable to keep passivity. The surface that rapidly increases the TiOOH fraction and donor density growth may be vulnerable even at low corrosion current.

4. Scope and Reliability of the Interpretation

The numerical interpretation is applicable to Ti–6Al–4V that is immersed in artificial seawater having pH 8.2 ± 0.1 and $25 \pm 1\,^{\circ}\mathrm{C}$ with cathodic current density being 20 mA cm^{-2}. The charging times include 0, 1, 4, 8, and 12 h. Thus, the values of Φ and Ψ are specific to the aforementioned electrolyte, current density, temperature, alloy state, and sequence of charging times. It is not correct to regard the indices as universal constants that apply to all titanium alloys and all seawater conditions.

The advantage of the calculation is in the use of the following parameters that are combined in an appropriate way because the degradation of the passive film is a coupled transport phenomenon: electrochemical resistance, current response, semiconductor defect density, physical film thickness, and surface chemistry. The disadvantage of the approach is that the descriptors are derived from average measurements. The surface chemistry might differ locally at α/β interfaces, hydride-containing areas, polished surface topography, and clusters of defects. In addition, Mott–Schottky analysis gives an averaged response of donor density and not the image of defect density distribution.

The measurements on the spatial scale would enhance the local interpretation. Transmission electron microscopy could be used to detect the interface changes associated with hydride formation. Atom probe tomography could be used to detect the segregation of hydrogen and alloying elements close to the passive film. Scanning electrochemical microscopy and localized impedance mapping could be used to detect the regions with enhanced electrochemical reaction activity. Spatially resolved XPS or time-of-flight secondary ion mass spectrometry could be used to check whether TiOOH enrichment is uniform or occurs near microstructural heterogeneities. These techniques would help to understand how hydrogen concentration in $\alpha + \beta$ microstructure affects the film chemistry detected by the current analysis.

5. Conclusion

Hydrogen charging of Ti–6Al–4V in artificial seawater deteriorates the passive film due to coupled processes of hydroxylation, growth of semiconductor defects, film thinning, and electrochemical resistance loss. The deterioration is not related only to the reduction of the film thickness. After 12 h, the film thickness is reduced from 1.81 to 1.12 nm, while the polarization resistance is reduced significantly more and reaches the value of $2.86 \times 10^5\,\Omega\,\mathrm{cm}^2$ as opposed to the initial value of $1.93 \times 10^6\,\Omega\,\mathrm{cm}^2$. The resistance is decreased by 85.18%, thus indicating the change of transport properties of the film.

The current response demonstrates the increased electrochemical activity but not the depassivation. The corrosion current density is increased from 4.62×10^{-8} to 9.19×10^{-8} A cm^{-2}, while the passive current density is increased from 9.05×10^{-7} to 1.67×10^{-6} A cm^{-2}. These results do not mean that the material is depassivated; however, the numbers confirm the weakness of the film that allows more charge transport.

The information about chemistry and semiconductors explains the underlying mechanism of the passivity decay. The content of TiO_2 is decreased from 93.86% to 86.18%, TiOOH-related species are increased from 6.14% to 13.82%, and the donor density is increased from 4.22×10^{19} to 6.10×10^{19} cm^{-3}. The passive film is transformed from the tight TiO_2 layer to the film with hydroxylation and defects.

The integrated indices reflect the extent of the changes. The value of the passive-film integrity index is decreased from 1.000 to 0.086, while the barrier-disorder amplification factor is increased from 1.000 to 38.996. The contribution of the 8–12 h interval is 88.27% of the total increment of Ψ. This result indicates that the hydrogen charging for a long time causes the development of the disordered barrier at the late stage. Ti–6Al–4V is still passive after hydrogen charging, but its passive film becomes a highly transportable, hydroxylated, and electronically defective barrier.

Conflict of Interest

The author declares no conflict of interest.

References

[1] Gurrappa, I. J. M. C. (2003). Characterization of titanium alloy Ti-6Al-4V for chemical, marine and industrial applications. *Materials characterization, 51*(2-3), 131-139.

[2] Donachie, M. J. (2000). Titanium: a technical guide. ASM international.

[3] Leyens, C., & Peters, M. (Eds.). (2006). Titanium and titanium alloys: fundamentals and applications. Wiley-vch.

[4] Schutz, R. W. (2005). Corrosion of titanium and titanium alloys.

[5] Blackwood, D. J. (2003). Biomaterials: past successes and future problems. *Corrosion reviews, 21*(2-3), 97-124.

[6] Landolt, D. (2007). Corrosion and surface chemistry of metals. EPFL press.

[7] McCafferty, E. (2010). Introduction to corrosion science. Springer Science & Business Media.

[8] Macdonald, D. D. (1992). The point defect model for the passive state. *Journal of the Electrochemical Society, 139*(12), 3434-3449.

[9] Frankel, G. S. (1998). Pitting corrosion of metals: a review of the critical factors. *Journal of the Electrochemical society, 145*(6), 2186-2198.

[10] Jones, D. A. (1996). Principles and prevention of corrosion. (No Title).

[11] Revie, R. W., & Uhlig, H. H. (2025). Corrosion and corrosion control. John Wiley & Sons.

[12] Oriani, R. A. (1978). Hydrogen embrittlement of steels. *Annual review of materials science, 8*(1), 327-357.

[13] Tal-Gutelmacher, E., & Eliezer, D. (2005). The hydrogen embrittlement of titanium-based alloys. *Jom, 57*(9), 46-49.

[14] Fukai, Y. (2005). The metal-hydrogen system: basic bulk properties. Berlin, Heidelberg: Springer Berlin Heidelberg.

[15] Videm, K., Lamolle, S., Monjo, M., Ellingsen, J. E., Lyngstadaas, S. P., & Haugen, H. J. (2008). Hydride formation on titanium surfaces by cathodic polarization. *Applied Surface Science, 255*(5), 3011-3015.

[16] Orazem, M. E., & Tribollet, B. (2008). Electrochemical impedance spectroscopy. *New Jersey, 1*(906), 383-389.

[17] Scully, J. R. (2000). Polarization resistance method for determination of instantaneous corrosion rates. *Corrosion, 56*(2), 199-218.

[18] Kelly, R. G., Scully, J. R., Shoesmith, D., & Buchheit, R. G. (2002). Electrochemical techniques in corrosion science and engineering. CRC press.

[19] Brug, G. J., van den Eeden, A. L., Sluyters-Rehbach, M., & Sluyters, J. H. (1984). The analysis of electrode impedances complicated by the presence of a constant phase element. *Journal of electroanalytical chemistry and interfacial electrochemistry, 176*(1-2), 275-295.

[20] Hirschorn, B., Orazem, M. E., Tribollet, B., Vivier, V., Frateur, I., & Musiani, M. (2010). Determination of effective capacitance and film thickness from constant-phase-element parameters. *Electrochimica acta, 55*(21), 6218-6227.

[21] Mansfeld, F. (1995). Use of electrochemical impedance spectroscopy for the study of corrosion protection by polymer coatings. *Journal of applied electrochemistry, 25*(3), 187-202.

[22] Bard, A. J., Faulkner, L. R., & White, H. S. (2022). Electrochemical methods: fundamentals and applications. John Wiley & Sons.

[23] Di Quarto, F., Piazza, S., & Sunseri, C. (1993). The photoelectrochemistry of thin passive layers. Investigation of anodic oxide films on titanium metal. *Electrochimica acta, 38*(1), 29-35.

[24] Roh, B., & Macdonald, D. D. (2007). Effect of oxygen vacancies in anodic titanium oxide films on the kinetics of the oxygen electrode reaction. *Russian Journal of Electrochemistry, 43*(2), 125-135.

[25] Macdonald, D. D. (1992). The point defect model for the passive state. *Journal of the Electrochemical Society, 139*(12), 3434-3449.

[26] Hakiki, N. B., Boudin, S., Rondot, B., & Belo, M. D. C. (1995). The electronic structure of passive films formed on stainless steels. *Corrosion science, 37*(11), 1809-1822.

[27] Pourbaix, M. (1974). Atlas of electrochemical equilibria in aqueous solutions. (No Title).

[28] Marino, C. E., de Oliveira, E. M., Rocha-Filho, R. C., & Biaggio, S. R. (2001). On the stability of thin-anodic-oxide films of titanium in acid phosphoric media. *Corrosion Science, 43*(8), 1465-1476.

[29] Shibata, T., & Zhu, Y. C. (1995). The effect of film formation conditions on the structure and composition of anodic oxide films on titanium. *Corrosion Science, 37*(2), 253-270.

[30] Pan, J., Thierry, D., & Leygraf, C. (1996). Electrochemical impedance spectroscopy study of the passive oxide film on titanium for implant application. *Electrochimica Acta, 41*(7-8), 1143-1153.

[31] Pan, J., Thierry, D., & Leygraf, C. (1996). Electrochemical impedance spectroscopy study of the passive oxide film on titanium for implant application. *Electrochimica Acta, 41*(7-8), 1143-1153.

[32] Qiao, Y., Qin, Y., Zhou, H., Yang, L., Wang, X., Wang, Z., ... & Zou, J. (2024). Electrochemical hydrogen charging on corrosion behavior of Ti-6Al-4V alloy in artificial seawater. *Chinese Journal of Mechanical Engineering, 37*(1), 2.